Spatial and temporal variation of rod photoreceptor reflectance in the human retina

Robert F. Cooper,[1] Adam M. Dubis,[2] Ashavini Pavaskar,[1] Jungtae Rha,[3] Alfredo Dubra,[4,5] and Joseph Carroll[2,3,6,*]

[1]*Department of Biomedical Engineering, Marquette University, Milwaukee, WI 53233 USA*
[2]*Department of Cell Biology, Neurobiology and Anatomy, Medical College of Wisconsin, Milwaukee, WI 53226 USA*
[3]*Department of Ophthalmology, Medical College of Wisconsin, Milwaukee, WI 53226 USA*
[4]*Flaum Eye Institute, University of Rochester, Rochester, NY 14642 USA*
[5]*Center for Visual Science, University of Rochester, Rochester, NY 14627 USA*
[6]*Department of Biophysics, Medical College of Wisconsin, Milwaukee WI 53226 USA*
**jcarroll@mcw.edu*

Abstract: Using adaptive optics imaging tools to image the living retina, numerous investigators have reported temporal fluctuation in the reflectivity of individual cone photoreceptors. In addition, there is cone-to-cone (spatial) variation in reflectivity. As it has only recently become possible to image the complete rod photoreceptor mosaic in the living human retina, we sought to characterize the reflectivity of individual rods and compare their behavior to that of foveal/parafoveal cones. Across two subjects, we were able to successfully track the reflectance behavior of 1,690 rods and 1,980 cones over 12 hours. Rod and cone photoreceptors showed similar regional and temporal variability in their reflectance profiles, suggesting the presence of a common governing physiological process. Within the rod and cone mosaics, there was no sign of spatial clumping of reflectance profile behavior; that is, the arrangement of cells of a given archetypal reflectance profile within the mosaic was indistinguishable from random. These data demonstrate the ability to track the behavior of rod reflectivity over time. Finally, as these and other reflectance changes may be an indicator of photoreceptor function, a future extension of this method will be to analyze this behavior in patients with rod photoreceptor dysfunction (*e.g.*, retinitis pigmentosa, Usher's syndrome, and congenital stationary night blindness).

OCIS codes: (110.1080) Active or adaptive optics; (170.2655) Functional monitoring and imaging; (170.3880) Medical and biological imaging; (330.7331) Visual optics, receptor optics; (330.5310) Vision-photoreceptors

References and links

1. D. T. Miller, D. R. Williams, G. M. Morris, and J. Liang, "Images of cone photoreceptors in the living human eye," Vision Res. **36**(8), 1067–1079 (1996).
2. A. R. Wade and F. W. Fitzke, "In vivo imaging of the human cone-photoreceptor mosaic using a confocal laser scanning ophthalmoscope," Lasers and Light in Ophthalmology **8**, 129–136 (1998).
3. J. Liang, D. R. Williams, and D. T. Miller, "Supernormal vision and high-resolution retinal imaging through adaptive optics," J. Opt. Soc. Am. A **14**(11), 2884–2892 (1997).
4. H. Hofer, L. Chen, G. Y. Yoon, B. Singer, Y. Yamauchi, and D. R. Williams, "Improvement in retinal image quality with dynamic correction of the eye's aberrations," Opt. Express **8**(11), 631–643 (2001).
5. A. Roorda, F. Romero-Borja, W. Donnelly Iii, H. Queener, T. J. Hebert, and M. C. W. Campbell, "Adaptive optics scanning laser ophthalmoscopy," Opt. Express **10**(9), 405–412 (2002).
6. Y. Zhang, B. Cense, J. Rha, R. S. Jonnal, W. Gao, R. J. Zawadzki, J. S. Werner, S. Jones, S. Olivier, and D. T. Miller, "High-speed volumetric imaging of cone photoreceptors with adaptive optics spectral-domain optical coherence tomography," Opt. Express **14**(10), 4380–4394 (2006).
7. J. L. Duncan, Y. Zhang, J. Gandhi, C. Nakanishi, M. Othman, K. E. Branham, A. Swaroop, and A. Roorda, "High-resolution imaging with adaptive optics in patients with inherited retinal degeneration," Invest. Ophthalmol. Vis. Sci. **48**(7), 3283–3291 (2007).
8. T. Y. Chui, H. Song, and S. A. Burns, "Adaptive-optics imaging of human cone photoreceptor distribution," J. Opt. Soc. Am. A **25**(12), 3021–3029 (2008).

#150009 - $15.00 USD Received 29 Jun 2011; revised 5 Aug 2011; accepted 8 Aug 2011; published 11 Aug 2011

9. E. J. Fernández, B. Hermann, B. Považay, A. Unterhuber, H. Sattmann, B. Hofer, P. K. Ahnelt, and W. Drexler, "Ultrahigh resolution optical coherence tomography and pancorrection for cellular imaging of the living human retina," Opt. Express **16**(15), 11083–11094 (2008).
10. R. J. Zawadzki, S. S. Choi, A. R. Fuller, J. W. Evans, B. Hamann, and J. S. Werner, "Cellular resolution volumetric in vivo retinal imaging with adaptive optics-optical coherence tomography," Opt. Express **17**(5), 4084–4094 (2009).
11. O. P. Kocaoglu, S. C. Lee, R. S. Jonnal, Q. Wang, A. E. Herde, J. C. Derby, W. Gao, and D. T. Miller, "Imaging cone photoreceptors in three dimensions and in time using ultrahigh resolution optical coherence tomography with adaptive optics," Biomed. Opt. Express **2**(4), 748–763 (2011).
12. A. Roorda and D. R. Williams, "Optical fiber properties of individual human cones," J. Vis. **2**(5), 4 (2002).
13. A. Pallikaris, D. R. Williams, and H. Hofer, "The reflectance of single cones in the living human eye," Invest. Ophthalmol. Vis. Sci. **44**(10), 4580–4592 (2003).
14. M. Pircher, J. S. Kroisamer, F. Felberer, H. Sattmann, E. Götzinger, and C. K. Hitzenberger, "Temporal changes of human cone photoreceptors observed in vivo with SLO/OCT," Biomed. Opt. Express **2**(1), 100–112 (2011).
15. J. Rha, R. S. Jonnal, K. E. Thorn, J. Qu, Y. Zhang, and D. T. Miller, "Adaptive optics flood-illumination camera for high speed retinal imaging," Opt. Express **14**(10), 4552–4569 (2006).
16. R. S. Jonnal, J. R. Besecker, J. C. Derby, O. P. Kocaoglu, B. Cense, W. Gao, Q. Wang, and D. T. Miller, "Imaging outer segment renewal in living human cone photoreceptors," Opt. Express **18**(5), 5257–5270 (2010).
17. R. S. Jonnal, J. Rha, Y. Zhang, B. Cense, W. Gao, and D. T. Miller, "In vivo functional imaging of human cone photoreceptors," Opt. Express **15**(24), 16141–16160 (2007).
18. K. Grieve and A. Roorda, "Intrinsic signals from human cone photoreceptors," Invest. Ophthalmol. Vis. Sci. **49**(2), 713–719 (2008).
19. J. Rha, B. Schroeder, P. Godara, and J. Carroll, "Variable optical activation of human cone photoreceptors visualized using a short coherence light source," Opt. Lett. **34**(24), 3782–3784 (2009).
20. C. J. Wolsley, K. J. Saunders, G. Silvestri, and R. S. Anderson, "Comparing mfERGs with estimates of cone density from in vivo imaging of the photoreceptor mosaic using a modified Heidelberg retina tomograph," Vision Res. **50**(15), 1462–1468 (2010).
21. H. Gao and J. G. Hollyfield, "Aging of the human retina. Differential loss of neurons and retinal pigment epithelial cells," Invest. Ophthalmol. Vis. Sci. **33**(1), 1–17 (1992).
22. C. A. Curcio, "Photoreceptor topography in ageing and age-related maculopathy," Eye (Lond.) **15**(3), 376–383 (2001).
23. C. A. Curcio, C. L. Millican, K. A. Allen, and R. E. Kalina, "Aging of the human photoreceptor mosaic: evidence for selective vulnerability of rods in central retina," Invest. Ophthalmol. Vis. Sci. **34**(12), 3278–3296 (1993).
24. C. A. Curcio, C. Owsley, and G. R. Jackson, "Spare the rods, save the cones in aging and age-related maculopathy," Invest. Ophthalmol. Vis. Sci. **41**(8), 2015–2018 (2000).
25. D. A. Newsome, "Retinitis pigmentosa, Usher's syndrome, and other pigmentary retinopathies," in *Retinal dystrophies and degenerations*, D. A. Newsome, ed. (Raven Press, New York, 1988), pp. 161–194.
26. E. L. Berson, "Retinitis pigmentosa. The Friedenwald Lecture," Invest. Ophthalmol. Vis. Sci. **34**(5), 1659–1676 (1993).
27. J. Carroll, S. S. Choi, and D. R. Williams, "In vivo imaging of the photoreceptor mosaic of a rod monochromat," Vision Res. **48**(26), 2564–2568 (2008).
28. J. Carroll, E. Banin, D. M. Hunt, R. Martin, M. Michaelides, L. Mizrahi-Meissonnier, A. T. Moore, D. Sharon, D. R. Williams, and A. Dubra, "Evaluating the photoreceptor mosaic in blue cone monochromacy (BCM)," Investigative Ophthalmology & Visual Science **51**, E-Abstract 2935 (2010).
29. N. Doble, S. S. Choi, J. L. Codona, J. Christou, J. M. Enoch, and D. R. Williams, "In vivo imaging of the human rod photoreceptor mosaic," Opt. Lett. **36**(1), 31–33 (2011).
30. A. Dubra and Y. Sulai, "Reflective afocal broadband adaptive optics scanning ophthalmoscope," Biomed. Opt. Express **2**(6), 1757–1768 (2011).
31. A. Dubra, Y. Sulai, J. L. Norris, R. F. Cooper, A. M. Dubis, D. R. Williams, and J. Carroll, "Noninvasive imaging of the human rod photoreceptor mosaic using a confocal adaptive optics scanning ophthalmoscope," Biomed. Opt. Express **2**(7), 1864–1876 (2011).
32. A. Dubra and Z. Harvey, "Registration of 2D images from fast scanning ophthalmic instruments," in *Biomedical Image Registration* (Springer, Heidelberg, 2010), pp. 60–71.
33. K. Y. Li and A. Roorda, "Automated identification of cone photoreceptors in adaptive optics retinal images," J. Opt. Soc. Am. A **24**(5), 1358–1363 (2007).
34. Q. V. Hoang, R. A. Linsenmeier, C. K. Chung, and C. A. Curcio, "Photoreceptor inner segments in monkey and human retina: mitochondrial density, optics, and regional variation," Vis. Neurosci. **19**(04), 395–407 (2002).
35. P. J. Diggle, *Statistical Analysis of Spatial Point Patterns*, Mathematics in Biology (Academic Press, London, 1983).
36. A. Roorda, A. B. Metha, P. Lennie, and D. R. Williams, "Packing arrangement of the three cone classes in primate retina," Vision Res. **41**(10-11), 1291–1306 (2001).
37. H. Hofer, J. Carroll, J. Neitz, M. Neitz, and D. R. Williams, "Organization of the human trichromatic cone mosaic," J. Neurosci. **25**(42), 9669–9679 (2005).
38. W. J. Kimberling and C. Möller, "Clinical and molecular genetics of Usher syndrome," J. Am. Acad. Audiol. **6**(1), 63–72 (1995).
39. E. Malm, V. Ponjavic, C. Möller, W. J. Kimberling, E. S. Stone, and S. Andréasson, "Alteration of rod and cone function in children with Usher syndrome," Eur. J. Ophthalmol. **21**(1), 30–38 (2011).

#150009 - $15.00 USD Received 29 Jun 2011; revised 5 Aug 2011; accepted 8 Aug 2011; published 11 Aug 2011

40. R. S. Molday, "Photoreceptor membrane proteins, phototransduction, and retinal degenerative diseases. The Friedenwald Lecture," Invest. Ophthalmol. Vis. Sci. **39**(13), 2491–2513 (1998).
41. I. Perrault, J. M. Rozet, S. Gerber, I. Ghazi, C. Leowski, D. Ducroq, E. Souied, J. L. Dufier, A. Munnich, and J. Kaplan, "Leber congenital amaurosis," Mol. Genet. Metab. **68**(2), 200–208 (1999).
42. S. P. Daiger, S. J. Bowne, and L. S. Sullivan, "Perspective on genes and mutations causing retinitis pigmentosa," Arch. Ophthalmol. **125**(2), 151–158 (2007).
43. K. M. Nishiguchi, M. A. Sandberg, N. Gorji, E. L. Berson, and T. P. Dryja, "Cone cGMP-gated channel mutations and clinical findings in patients with achromatopsia, macular degeneration, and other hereditary cone diseases," Hum. Mutat. **25**(3), 248–258 (2005).

1. Introduction

In examining the first direct *in vivo* images of the human cone mosaic, one of the more salient features of the appearance of individual cone photoreceptors is that they vary considerably in their reflectance [1,2]. With the advent of ophthalmic adaptive optics (AO) [3,4], it has become almost routine to non-invasively obtain images of the cone mosaic. Regardless of the AO imaging modality used (scanning laser ophthalmoscope, fundus camera, or optical coherence tomography), similar regional variation in the appearance of cones has been seen in the corresponding *in vivo* images of the cone mosaic [5–13]. By measuring the Stiles-Crawford effect of individual cones using an AO fundus camera, it was shown that this spatial variability is not caused by cone-to-cone differences in directional tuning [12,13]. However despite being a universal feature of images of the cone mosaic, the origin of the cell to cell variability in cone reflectance remains unclear.

Besides exhibiting variability in reflectivity between different cones, individual cones also vary in their reflectivity over time, on scales ranging from seconds to hours [13–15]. These changes occur both in the presence and absence of a stimulus, and it has been suggested that these changes reflect physiological activity within the photoreceptor. For example, using a flood-illuminated AO fundus camera, Pallikaris *et al.* suggested that long-term variation in cone reflectivity could be due to the process of disc shedding [13]. Recently, Pircher *et al.* [14] and Jonnal *et al.* [16] provided data suggesting that the longer term temporal changes in cone reflectivity are due to the outer segment renewal process. In contrast, rapid changes in reflectivity can be seen in response to stimulation with light [17–19], and it has been suggested that these rapid changes in cone reflectivity measured *in vivo* are related to the phototransduction process [17]. The clinical applications of such measurements could be substantial; with the ability to monitor cone structure and function, researchers would be positioned to elucidate more clearly the disease sequence of retinal degenerations, and also provide additional tools for assessing therapeutic efficacy in individuals receiving intervention.

The human retina has two classes of photoreceptor, cones and rods. While rods outnumber cones by nearly 20:1, cones have received considerably more attention in cellular retinal imaging, primarily due to their easy visualization, even without AO-equipped devices [1,2,14,20]. This is unfortunate, given the prominent role that rods play in aging [21–24] and devastating retinal degenerations [25,26]. In cases where rod dysfunction precedes that of the cones, the inability to image rod structure and function represents a significant barrier in bringing high-resolution imaging tools to bear on their management. Part of the difficulty in translating previous studies on the spatial and temporal properties of cones to the rod mosaic has simply been an inability to readily resolve rods in vivo. Besides a couple reports of rod visualization in the diseased retina [27,28], there had only been a single report of rod visualization in the normal retina. However, it was the result of significant image processing and enhancement, and provided only intermittent rod visualization [29]. Recently, we developed an AO scanning ophthalmoscope (AOSO) capable of imaging the contiguous rod photoreceptor mosaic [30,31]. Here we sought to investigate the spatial and temporal variation in reflectivity of the rod mosaic and compare its behavior to that previously observed for the cone photoreceptor mosaic.

#150009 - $15.00 USD Received 29 Jun 2011; revised 5 Aug 2011; accepted 8 Aug 2011; published 11 Aug 2011

2. Methods

2.1. Human subjects

One male (JC_0002, age 28 years, emmetrope) and one female (JC_0138, age 27 years, –1D myope) were recruited for the study. Neither of the subjects had any retinal pathology, though the male subject does have an inherited color vision defect (deuteranopia). All research followed the tenets of the Declaration of Helsinki, and study protocols were approved by the institutional research boards at the Medical College of Wisconsin and Marquette University. Subjects provided informed consent after the nature and possible consequences of the study were explained. Axial length measurements were obtained on both subjects using an IOL Master (Carl Zeiss Meditec, Dublin, CA) for scaling of the retinal images.

2.2. Imaging the photoreceptor mosaic

An AOSO was used to image each subject's photoreceptor mosaic. The AOSO is housed at the Medical College of Wisconsin, and system design details can be found elsewhere [30]. A 680nm superluminescent diode with a full-width at half-maximum (FWHM) bandwidth of 8.5nm from Superlum Ireland (Carrigtwohill, County Cork, Ireland), was used for reflectance retinal imaging. Assuming a refractive index of 1.43 for the cone outer segment, we estimate the coherence length of this source as 17 μm. The power incident on the cornea was 111.11 μW.

The subjects were each imaged at one-hour intervals beginning at 10am and ending at 10pm. Their right eye was dilated and accommodation suspended using one drop each of Phenylephrine Hydrochloride (2.5%) and Tropicamide (1%), and the drops were re-administered between each imaging session. A foveal and peripheral retinal location was selected for imaging and analysis: 0.5° temporal-superior from fixation, and 10° temporal from fixation, respectively. The field of view of the raw images was 0.95° x 0.95°. At each time point, a single image sequence was acquired at the foveal location, and six image sequences were taken at the 10° temporal location. The additional image sequences in the peripheral location were acquired to minimize the effects of any hourly fixation drift and ensure maximum overlap of the common image area. Individual image sequences contained 150 frames. Each image sequence was acquired within about 10 minutes from the start of each hour. Owing to the fact that the targeted image location was exposed to the imaging light (680 nm) even when we were not saving an image sequence, we estimate that at each time point the cones and rods were 100% and 70% bleached, respectively. For the remainder of each hour, the subject's visual activity was not limited and consisted mainly of reading and computer work. As such, other than the time spent acquiring images, each subject was exposed to normal indoor lighting conditions for the entire experiment duration of 12 hours.

2.3. Processing of AOSO image sequences

In order to correct for distortions in the retinal images due to the sinusoidal motion of the resonant optical scanner, we first estimated the distortion from images of a Ronchi ruling, and then re-sampled the images over a grid of equally spaced pixels. After this "desinusoiding", the movies were manually inspected to identify reference frame(s) with minimal distortion and maximal sharpness for subsequent registration using custom software [32]. Registration of frames within a given image sequence was performed using a "strip" registration method, in which the images were registered by dividing the image of interest into strips, aligning each strip to the location in the reference frame that maximizes the normalized cross correlation between them [32]. Once all the frames were registered, the 50 frames with the highest normalized cross correlation to the reference frame were averaged, in order to generate a final image with an increased signal to noise ratio (SNR) for subsequent analysis. For the peripheral imaging location, the multiple registered average images from each time point were manually inspected, and the image with maximum apparent overlap to the images from the other time points was selected for further processing and analysis.

#150009 - $15.00 USD Received 29 Jun 2011; revised 5 Aug 2011; accepted 8 Aug 2011; published 11 Aug 2011

For a given imaging location, the average images from each time point were registered to each other using an affine transformation (i2kRetina, Dual Align, LLC, Clifton Park, NY). This aligned image stack was then cropped to a common area, a reference frame was selected, and the image stack then went through strip registration as described above. Finally, the image series were normalized to the temporal mean of the nonzero portions of the stack. The movies, Fig. 1 and Fig. 2, display the result of these registrations for the foveal and peripheral imaging locations, respectively.

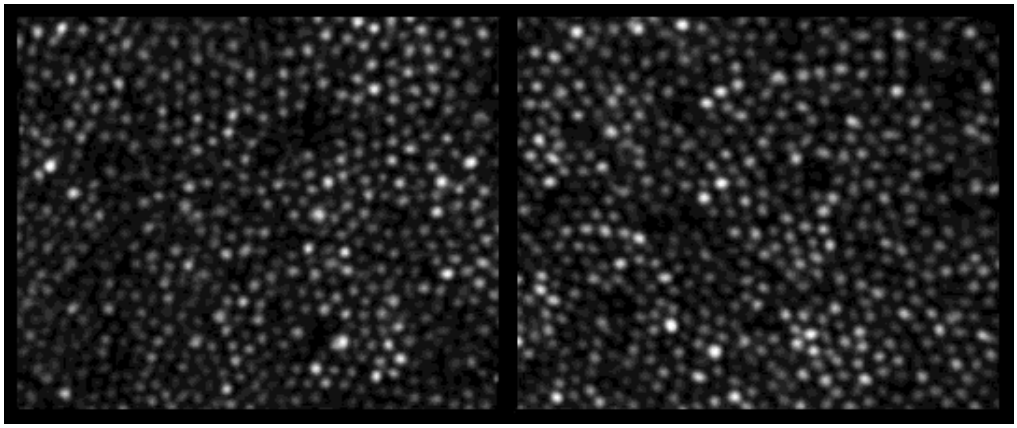

Fig. 1. Time-lapse video showing changes in cone reflectance at 0.5° temporal-superior over 12 hours for JC_0138 (*left*) and JC_0002 (*right*) (Media 1). Each image is 112 x 92 μm.

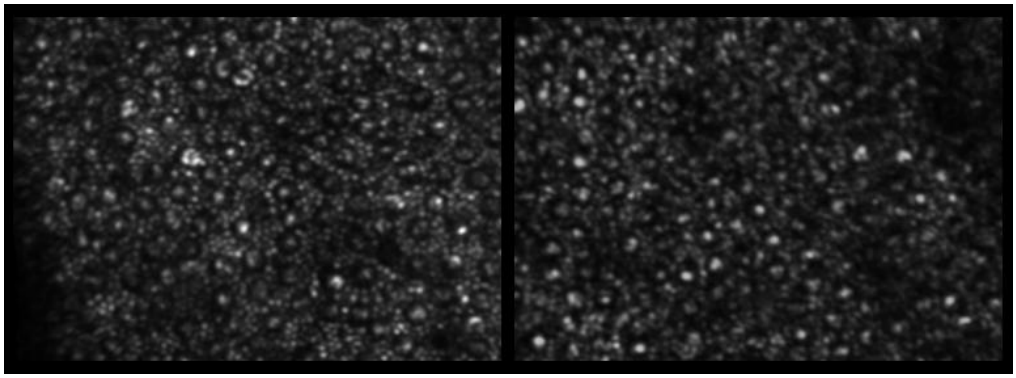

Fig. 2. Time-lapse video showing changes in rod reflectance at ~10° temporal over 12 hours for JC_0138 (*left*) and JC_0002 (*right*) (Media 2). Each image is 168 x 122 μm.

2.4. Generating reflectance profiles

To ensure we were selecting the center of a given cell, we first averaged the images from all 13 time points at each imaging location for both subjects, resulting in four composite images (Fig. 3 and Fig. 4). These images were then used to determine preliminary cone and rod coordinate locations. The position of foveal cones was identified using a modified version of previously described semi-automated algorithm, which also allowed manual addition/subtraction of cones missed or selected in error [33]. A total of 1,980 cones were selected for analysis using this method. The position of peripheral rods was determined by manual selection, and a total of 1,690 rods were selected for analysis. From these preliminary coordinates, the final coordinates were determined using custom Matlab (Mathworks, Natick, Massachusetts, USA) software that identified the local maximum within a 3x3 pixel (1.25x1.25 μm) region around the initial cone (or rod) coordinate. Owing to the increase in

#150009 - $15.00 USD Received 29 Jun 2011; revised 5 Aug 2011; accepted 8 Aug 2011; published 11 Aug 2011

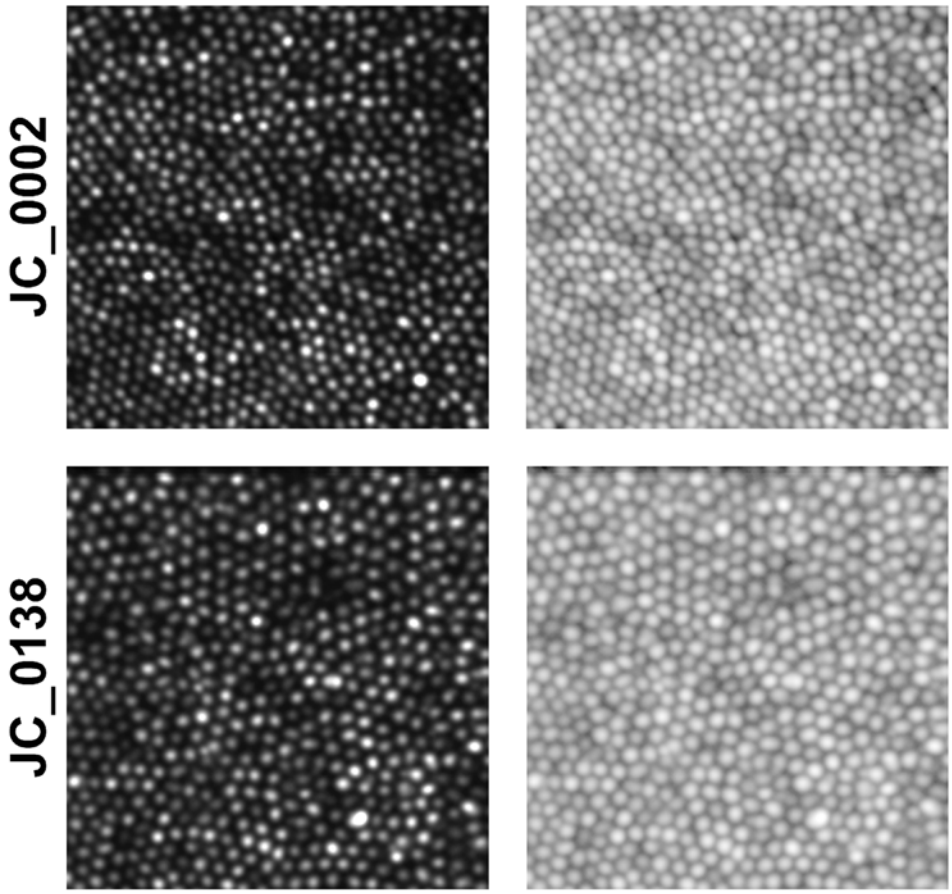

Fig. 3. Photoreceptor composite images for the foveal (0.5° temporal-superior) imaging locations. These images were created by aligning and averaging all 13 time points, and are shown using both a linear (*left*) and logarithmic (*right*) display.

cell diameter, multiple waveguide modes were present in the peripheral cone photoreceptors. This resulted in variability in the reflectance of individual peripheral cones within their cell boundary. In addition, the small number of cones (<50) present in the peripheral images would make any global conclusion about their reflectance behavior over time difficult. As such, we decided not to analyze the reflectivity of these peripheral cones.

The final coordinates were adjusted for each frame within the aligned image stack, in order to compensate for small errors in image registration. This was done by first projecting a mask for each cell through the aligned image stack. A square 3x3 pixel and circular 5 pixel diameter mask was used for rods and cones, respectively. For each frame, each cells' mask was repositioned to a local maximum, which never occurred greater than 1 pixel away from the original final coordinate. Reflectance profiles for every isolated cone and rod were generated by plotting reflectance as a function of time, where reflectance at a given time point is defined as the average intensity of all the pixels within the photoreceptor mask. For easier visualization of the behavior of individual cells, we normalized the reflectance values of each profile to the mean reflectance of that particular cell and then subtracted 1. This results in plots that effectively show the relative reflectance changes.

#150009 - $15.00 USD Received 29 Jun 2011; revised 5 Aug 2011; accepted 8 Aug 2011; published 11 Aug 2011

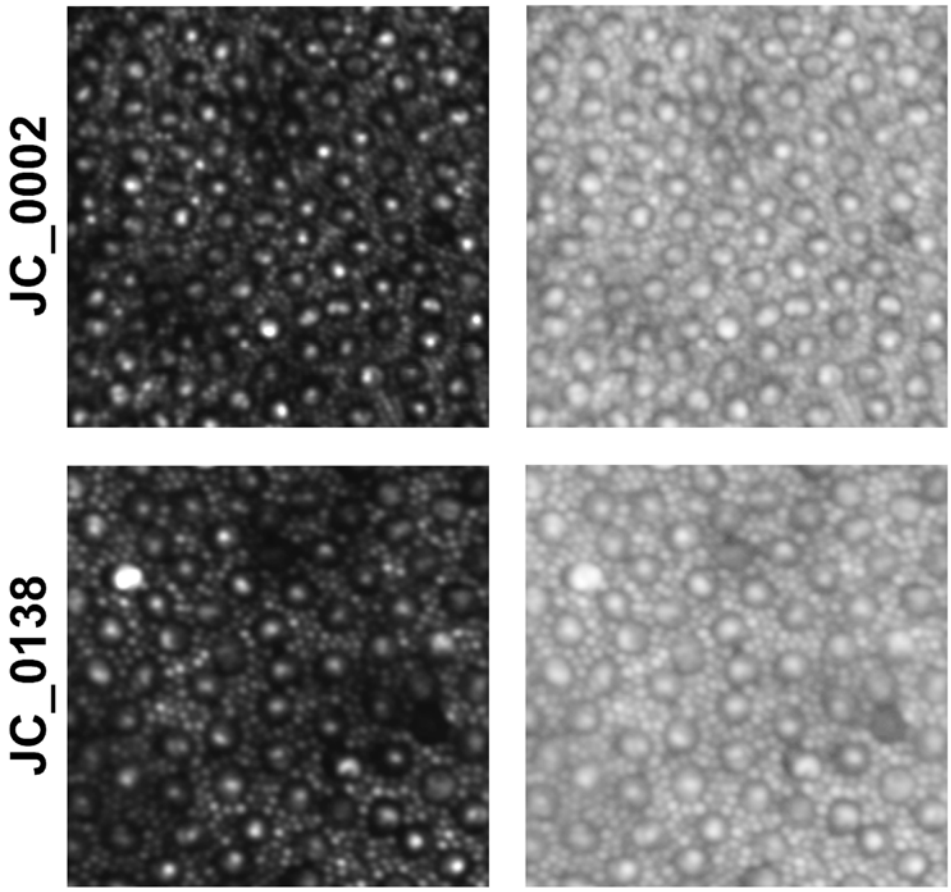

Fig. 4. Photoreceptor composite images for the peripheral (~10° temporal) imaging locations. These images were created by aligning and averaging all 13 time points, and are shown using both a linear (*left*) and logarithmic (*right*) display.

2.5. Analyzing reflectance profiles

Each cell type (rod/cone) was analyzed separately for each subject. To analyze the reflectance profiles for a given cell type, we determined the linear component (slope) of each profile by calculating the least squares linear fit of the profile. The mean and standard deviation of the slopes was calculated, and each cell was placed in one of two groups. Those with linear components that fell below 1 standard deviation from the mean were placed in the low slope group, and the remaining cells placed in the high slope group. Next, the linear component was removed from each profile and the standard deviation of the resultant signal was computed. The mean and standard deviation of the signal standard deviations for cells within each group was calculated. Cells having a signal standard deviation below 1 standard deviation from the mean for that group of cells were considered to have a linear reflectance profile, with the remaining cells regarded as having a fluctuating reflectance profile.

Further classification is possible, but is used for illustrative purposes only. For cells having a linear reflectance profile (top panels in Fig. 5 and Fig. 6**)**, the cells with low slope were considered flat while those with high slope were considered gradual. For cells having a fluctuating reflectance profile (bottom panels in Fig. 5 and Fig. 6), the cells with low slope were considered to have oscillatory profiles while those with high slope could be either oscillatory or abrupt. Among the high slope cells, those with the highest signal standard

#150009 - $15.00 USD Received 29 Jun 2011; revised 5 Aug 2011; accepted 8 Aug 2011; published 11 Aug 2011

deviation (greater than 1 standard deviation from the mean) were classified as abrupt and the remainder was classified as oscillatory, having signal standard deviations within 1 standard deviation of the mean. All statistical analysis was done using Instat (GraphPad Software, Inc., La Jolla, CA).

3. Results

3.1. Temporal variability of rod and cone photoreceptor reflectance

Inspection of the movies in Fig. 1 and Fig. 2 reveals remarkable temporal variability of the reflectance of individual cone and rod photoreceptors, respectively. Moreover, it is clear that not all cells are behaving the same way – some cells have multiple oscillations in their reflectance, while others showed no change in reflectance over the 12-hour experiment. This variation can be further appreciated in Fig. 5 and Fig. 6, which show normalized reflectance profiles for cones (JC_0002) and rods (JC_0138). The cells displayed were chosen so as to capture the range in archetypes observed. Using the classification scheme defined above, we

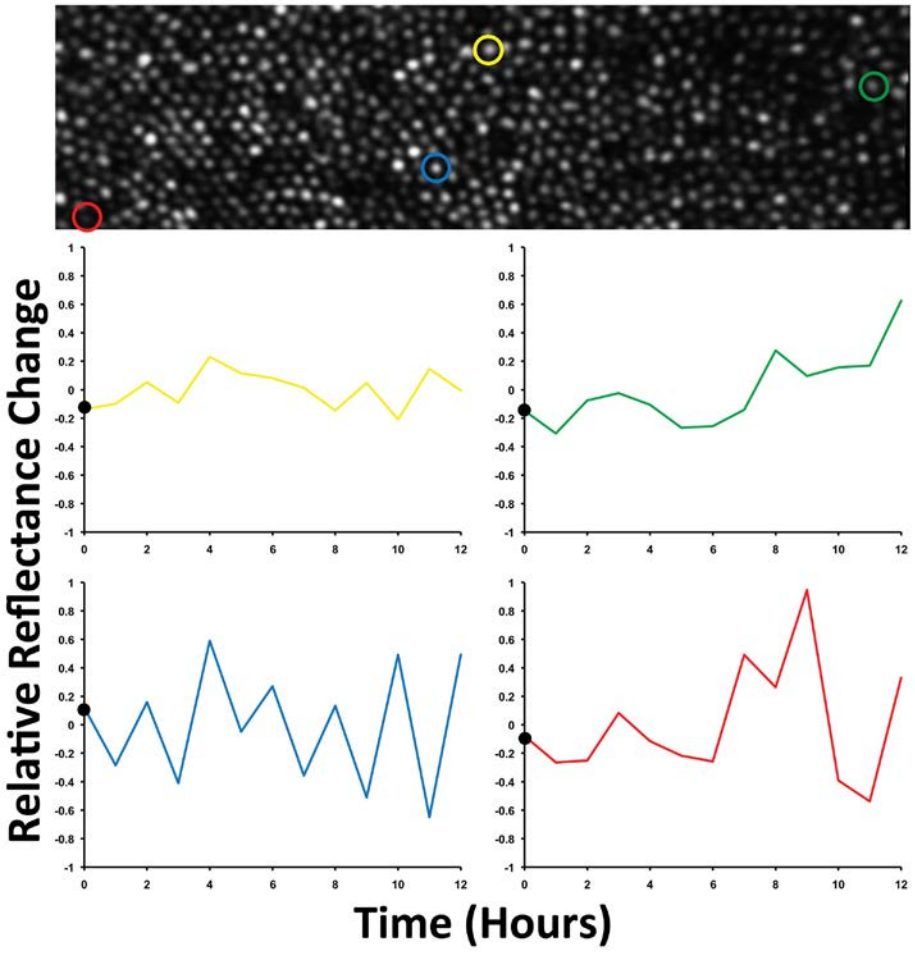

Fig. 5. Movie sequence of hourly AOSO images of the cone mosaic in JC_0002, showing representative normalized cone reflectance profiles (Media 3). The archetypes shown are flat (*top left*), gradual (*top right*), oscillatory (*bottom left*), or abrupt (*bottom right*). The circles in the retinal image are color coded to their respective profile plot, and their size was chosen for improved visualization and does not represent the area over which reflectance was analyzed.

#150009 - $15.00 USD Received 29 Jun 2011; revised 5 Aug 2011; accepted 8 Aug 2011; published 11 Aug 2011

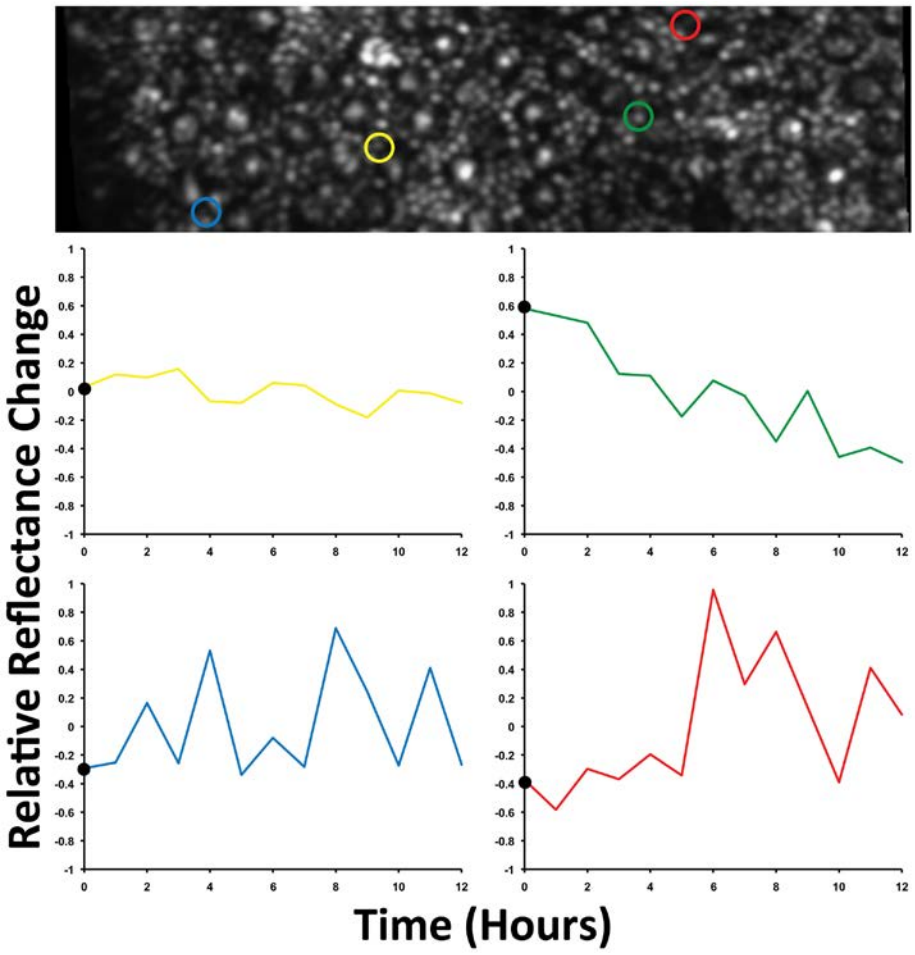

Fig. 6. Movie sequence of hourly AOSO images of the rod mosaic in JC_0138 showing representative normalized rod reflectance profiles (Media 4). The primary archetypes were flat (*top left*), gradual (*top right*), oscillatory (*bottom left*), or abrupt (*bottom right*). The circles in the retinal image are color coded to their respective profile plot, and their size was chosen for improved visualization and does not represent the area over which reflectance was analyzed.

found that for JC_0002, 15.6% of the cones and 13.5% of the rods had flat or gradual profiles, while for JC_0138, 16.1% of the cones and 13.7% of the rods had flat or gradual profiles. One could likely further refine the classification of these profiles by assessing the magnitude of the linear component, however subsequent thresholds on metrics like these would be subjective and not contribute further to the understanding of the biological basis of these reflectance changes. The conclusion from these data is that there is enormous variation in both cone and rod reflectivity over time.

3.2. Cell-to-cell variation of cone and rod reflectance

As mentioned earlier, one of the more prominent features in images of the cone mosaic is variation in the reflectivity of individual cones. While the origin of this variation is not fully understood, we examined whether the rod mosaic showed similar variation. At the 11am time point, we analyzed the distribution of the normalized reflectance values for the cones and rods for both subjects. Figure 7 shows the corresponding normalized histograms, and there was substantial variation in both cell types. For the cones, the standard deviation was 52% of the

#150009 - $15.00 USD Received 29 Jun 2011; revised 5 Aug 2011; accepted 8 Aug 2011; published 11 Aug 2011

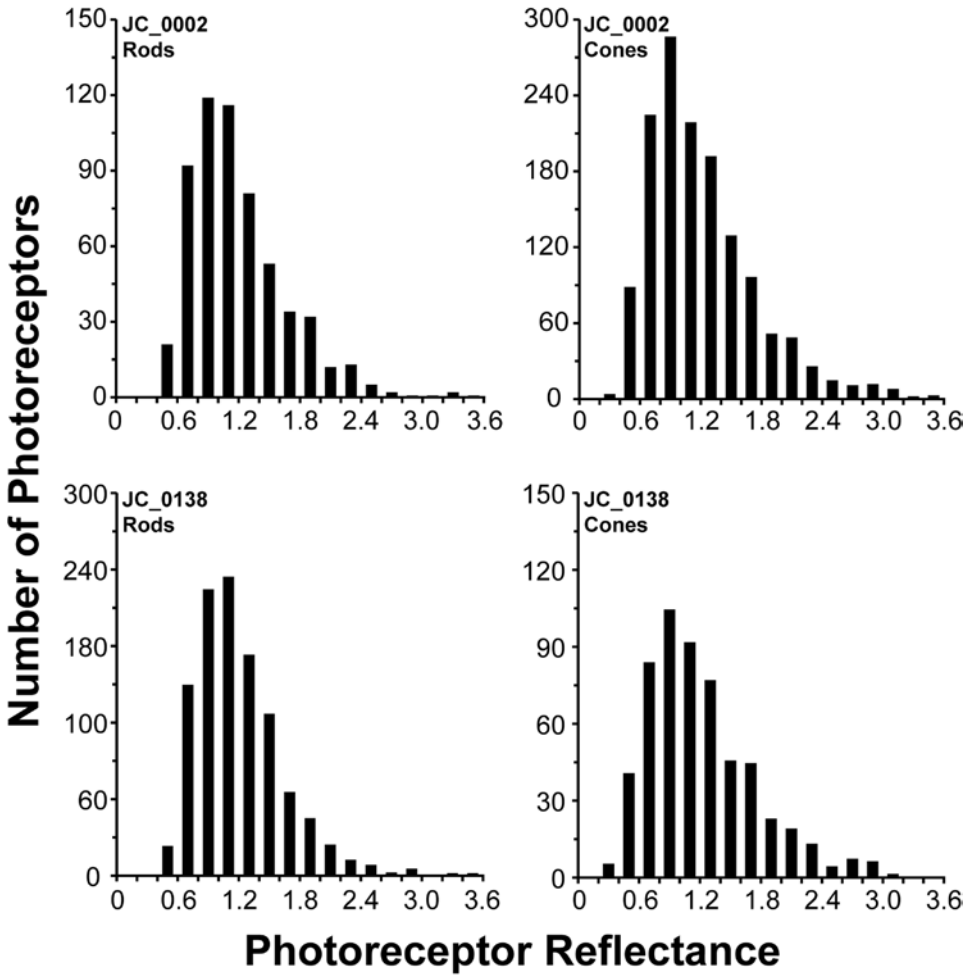

Fig. 7. Histogram of normalized reflectance of the cone and rod photoreceptor mosaics, for the 11am time point. Both the rods and cones each show significant variation in reflectivity, and similar results were observed at the other time points. This figure corrected August 15, 2011.

mean for both JC_0138 and JC_0002. For the rods, the standard deviation was 42% of the mean for JC_0138 and 48% of the mean for JC_0002. For each subject, the rods were found to have a significantly lower standard deviation that the cones (JC_0002, $p = 0.0246$; JC_0138, $p<0.0001$). One explanation for the rods being apparently less variable is that the rods had an overall lower reflectivity than the cones (JC_0002; cones = 61.74 a.u., rods = 38.16 a.u., $p<0.0001$, Mann-Whitney test; JC_0138; cones = 61.91 a.u., rods = 50.47 a.u., $p<0.0001$, Mann-Whitney test). Despite initially setting the gain of the PMT's to provide roughly equal mean pixel intensity for the foveal and peripheral imaging locations, the peripheral cones appear to have driven the behavior of the overall image intensity. This leaves the rods as being dimmer on average and may account for their apparently lower standard deviation. A second factor to consider is that rods and cones have different morphology [34], which of course would be expected to contribute to their waveguide behavior. Regardless, the general behavior of substantial inter-cell variation in reflectivity that has been well documented in cones appears to exist in the rods as well.

#150009 - $15.00 USD Received 29 Jun 2011; revised 5 Aug 2011; accepted 8 Aug 2011; published 11 Aug 2011

3.2. Spatial analysis of cell classification

As we identified each cell as having a linear or fluctuating reflectivity profile, we could examine whether the two submosaics were distributed randomly, or whether there was any tendency for cells belonging to the same submosaic to be near each other. This analysis was done using a previously described technique [35], which uses information about the photoreceptor mosaic on all spatial scales and has been used to examine the relative arrangement of long- and middle-wavelength sensitive cones within the trichromatic cone mosaic [36,37]. The distances between each cell having a linear reflectance profile and every other cell having a linear reflectance profile was calculated, and a cumulative histogram of intercell distances was generated. Monte Carlo simulations (n = 1000) were used to compute the expected cumulative histogram of intercell distances in a random arranged mosaic. These random mosaics were generated by taking the (x,y) coordinates of all of the cells and randomly assigning a constant fraction of them to be linear. The average, minimum, and maximum cumulative histograms were calculated and compared to the actual cumulative histogram for that particular group of cells. Figure 8 shows cumulative histogram comparisons

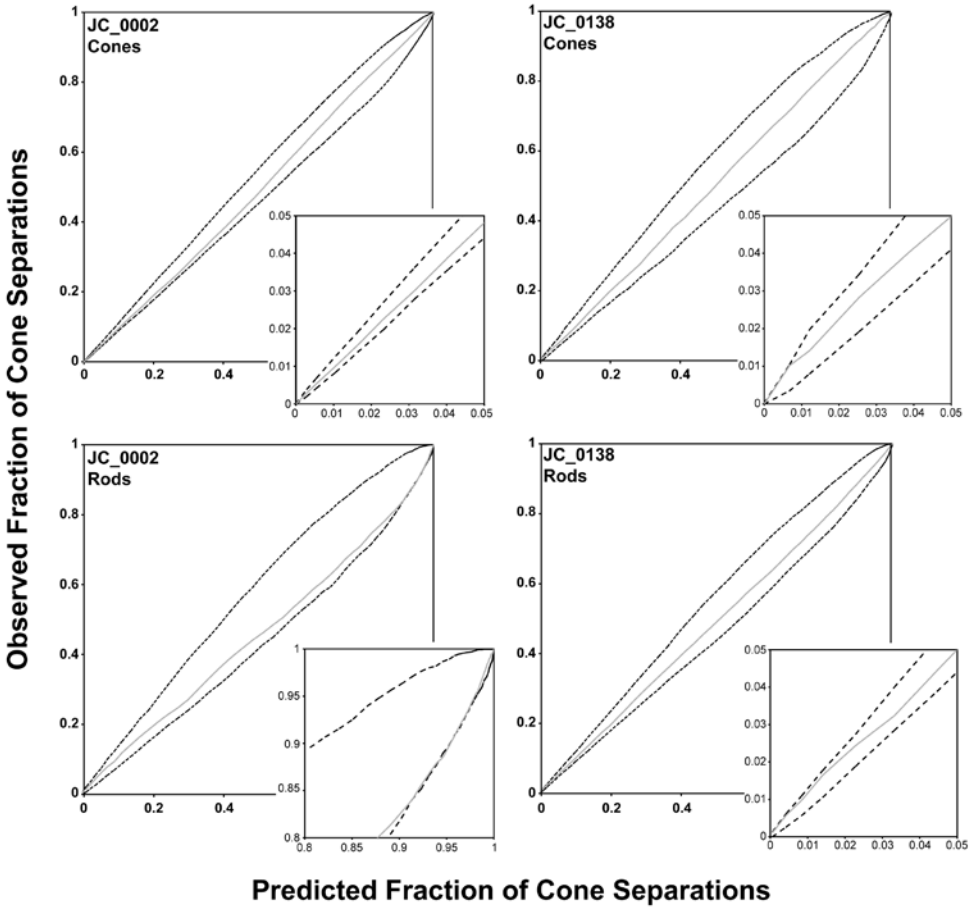

Fig. 8. Cumulative histogram comparison (CHC) plots for the linear reflectance profile cells. In each plot, the solid line represents the fraction of intercell separations within a given distance for the actual cone or rod mosaic versus that for the average of 1000 random simulations. The minimum and maximum bounds of these simulations is given as the dashed lines. The insets show areas of the CHC plots where the actual data approaches or exceeds the bounds of the random simulations.

#150009 - $15.00 USD Received 29 Jun 2011; revised 5 Aug 2011; accepted 8 Aug 2011; published 11 Aug 2011

(CHC) for all four data sets. The arrangement of the cells having linear reflectivity profiles within the overall cone (or rod) mosaic is indistinguishable from random for three of the four data sets, as evident by the fact that the CHC plot for the actual data does not fall outside of the minimum or maximum bounds of the random simulations. The rod mosaic of JC_0002 has a slight bias towards clumping (as the CHC inset reveals fewer large inter-rod distances compared to that of the random simulations). It was previously shown that a slight bias towards clumping of cones of like spectral subtype (long- or middle-wavelength sensitive) could be attributed to residual optical blur [36,37], and it may be that optical blur in our images also affects our analysis. As such, we conclude that the arrangement of cells having linear reflectivity profiles within the overall mosaic can be considered indistinguishable from random.

4. Discussion

We successfully imaged the rod and cone photoreceptor mosaic over 12 hours using an AOSO. By registering images from different time points, we were able to track the reflectance behavior of individual rod and cone photoreceptors over time. As has been shown previously for cones, we find that individual rods vary in their reflectance over time. This suggests that a common physiological mechanism underlies this phenomenon. Moreover, at a given moment in time, the rod mosaic showed remarkable variation in rod-to-rod reflectivity, which has also been observed for the cone mosaic [1,2]. The origin of the cell-cell variation remains to be elucidated; however our data would also suggest a common mechanism behind this feature of the rod and cone mosaics. Interestingly, our data reveal no tendency for neighboring cells to have the same reflectance profile behavior. As we develop techniques to further classify cells into additional archetypes, it will be interesting to re-examine the spatial arrangement of cells of like type.

There were a number of limitations of the current study. First, the results are based on only two subjects, though there is no reason to think that the findings do not represent a universal property of the healthy human rod photoreceptor mosaic. Second, a relatively coarse sampling (hourly) was used. Future experiments using finer time sampling are needed to better characterize the temporal variation of rod photoreceptors reflectance. Along these lines, it is worth noting that our classification scheme is rather arbitrary, but nevertheless illustrates the significant variability in reflectivity profiles among cones and rods.

Previous studies have suggested that differences in cone reflectivity observed in AO images are due to differences in the length of the outer segment [16,17]. Specifically, it has been suggested that sinusoidal reflectance oscillations can only be observed when using imaging sources with coherence lengths longer than that of the outer segment. However, both our results and those of Pallikaris *et al*. [13], resulting from using light sources with coherence lengths shorter than twice the length of a photoreceptor outer segment, strongly indicate that fluctuations in photoreceptor reflectivity are not only attributable to interference between light reflected at opposite ends of the outer segments. It is plausible that local sub-cellular changes at either the anterior or posterior end of the outer segment contribute to the overall reflectance profile. More importantly, the reflectivity fluctuations reported in these studies, which notably using different imaging modalities, are an order of magnitude larger than those reported in [16] and [17], and of a more complex temporal behavior. The important point is that complete characterization of the origin of these reflectance changes will require the use of short and long coherence length sources.

Regardless of the exact origin of the reflectance changes observed here, the fact remains that they appear to be similar in both cones and rods – suggesting a common physiological process. Thus, examination of temporal variation of photoreceptor reflectance may provide a means for assessing relative rod photoreceptor health in aging and in retinal disease. If temporal reflectance fluctuation is a property of all photoreceptors in “normal” retina, then it follows that pathological retina may exhibit altered characteristics. Of particular interest would be examining patients who have defects in ciliary trafficking of proteins from the inner segment to the outer segment [38,39]. Also of interest (and likely to be of more use clinically)

#150009 - $15.00 USD Received 29 Jun 2011; revised 5 Aug 2011; accepted 8 Aug 2011; published 11 Aug 2011

are the optical reflectance changes of rods and cones in response to photic stimulation. Previous reports have suggested that this behavior may have its origin in the phototransduction cascade [17]. The plethora of human mutations that selectively impair different components of the phototransduction cascade [40–43], combined with our ability to track the behavior of individual rods (and cones) over time, provides a unique opportunity to dissect, *in vivo*, the origin of these optical phenomena.

5. Acknowledgments

Joseph Carroll is the recipient of a Career Development Award from Research to Prevent Blindness. Alfredo Dubra-Suarez, Ph.D., holds a Career Award at the Scientific Interface from the Burroughs Welcome Fund. This research was supported by the National Institutes of Health (R01EY014375, P30EY001319, P30EY001931, R01EY017607 and T32EY014537). Funding was also provided by the E. Matilda Ziegler Foundation for the Blind, Hope for Vision, and unrestricted grants from Research to Prevent Blindness. Part of this investigation was conducted in a facility constructed with support from the Research Facilities Improvement Program, from the National Center for Research Resources, NIH, grant number C06 RR-RR016511. The authors would like to thank Zach Harvey and Brett Schroeder for their assistance with imaging and software support. We thank Austin Roorda and Ben Masella for assistance with photopigment bleaching calculations.

Publisher's note: Figure 7 was corrected postpublication on August 15, 2011.

#150009 - $15.00 USD Received 29 Jun 2011; revised 5 Aug 2011; accepted 8 Aug 2011; published 11 Aug 2011